The Influence of Vortex Sheet Geometry on the Kelvin-Helmholtz Instability

Ryan Murray & Galen Wilcox*
North Carolina State University, Raleigh, NC, 27606, USA

November 8, 2022

Abstract

This article revisits the instability of sharp shear interfaces in incompressible fluids, which are also called vortex sheets. We study the Birkhoff-Rott equation, which describes the motion of vortex sheets according to the incompressible Euler equations in two dimensions. The classical Kelvin-Helmholtz instability demonstrates that an infinite, flat vortex sheet has a strong linear instability. We show that this is not the case for vortex sheets which are circular: such a configuration is linearly stable, and is the first example of a linearly stable solution to the Birkhoff-Rott equation. We subsequently derive a sufficient condition for linear instability of a circular vortex sheet for a family of generalized Birkhoff-Rott kernels, and show that a common regularized kernel used in numerics and analysis destabilizes the circular vortex sheet. Finally, we show experimental results which qualitatively match the types of instabilities that are observed numerically.

1 Introduction

Sharp shear interfaces are a common phenomenon in many fluid dynamics problems. These shear interfaces, which are characterized by a mismatch of tangential velocities along a surface (in three dimensions) or a curve (in two dimensions), appear in wakes, jets, and atmospheric dynamics. Indeed, one can argue that in many of these applications the most relevant fluid behavior is described by this shear interface.

In the context of inviscid flow, the simplest example of such an interface is the flat vortex sheet in two dimensions, whose velocity is given by

$$u_{KH}(x,t) \equiv u_{KH}(x) = \begin{cases} (u^+, 0) & \text{for } x_2 > 0 \\ (u^-, 0) & \text{for } x_2 < 0 \end{cases}.$$

*Authors ordered alphabetically

Due to the discontinuity along the surface $x_2 = 0$ this velocity field is not a classical solution of the incompressible Euler equation

$$\partial_t u + \nabla u \cdot u = \nabla p, \qquad \nabla \cdot u = 0.$$

However, by rewriting this equation in terms of the vorticity $\omega = \nabla \times u$, we arrive at the system

$$\begin{aligned} &\partial_t \omega + u \cdot \nabla \omega = 0, \\ &u = \int K(x-y)\omega(y)dy, \\ &K(z) := -\frac{1}{2\pi}(-z_2/|z|, z_1/|z|). \end{aligned} \tag{1.1}$$

Equation (1.1) can be interpreted to mean that the vorticity is purely advected by the velocity field in two-dimensions, and that the velocity is determined by a non-local linear operator, namely the Biot-Savart law, acting on the vorticity. This is known as the vorticity-stream formulation of the Euler equation.

The vorticity-stream formulation admits a very weak interpretation in which vorticities are permitted to be measures as opposed to only functions. Such a formulation is both mathematically elegant and applicable to many model flows, such as point vortices, vortex patches, and vortex sheets. In particular, the steady flow u_{KH} corresponds to a vorticity which is a measure supported on the line $x_2 = 0$, or more precisely $\omega(A) = c_0 \mathcal{H}^1(A \cap \{x_2 = 0\})$, with $c_0 = (u^- - u^+)$.

There has been a significant body of work attempting to describe the evolution of shear interfaces in fluids. In particular, if vorticity is supported along a curve $z : [a, b] \times [t_0, t_1] \to \mathbb{C} \sim \mathbb{R}^2$, parametrized by vorticity density, then by manipulating Equation (1.1) one may arrive at the Birkhoff-Rott equation

$$\partial_t z^*(\alpha, t) = \frac{1}{2\pi i} \text{P.V.} \int_a^b \frac{1}{z(\alpha, t) - z(\beta, t)} \, d\beta, \tag{1.2}$$

where P.V. denotes the principal value integral, which is necessitated by the order of the singularity in the integrand as $\beta \to \alpha$. We will let $(\cdot)^*$ denote the complex conjugate throughout the paper. For simplicity in this work we only consider curves under which $z(a) = z(b)$ when a, b are finite, or the situation where $[a, b] = \mathbb{R}$. A derivation of this equation from the Euler equation can be found in [41]. A major motivation for studying the Birkhoff-Rott equation is that one can ignore the dynamics away from shear interfaces, which are likely themselves unstable, and instead focus on a simpler curve evolution equation. Indeed the Birkhoff-Rott equation is observed to admit, with varying degrees of rigor, self-similar spiral solutions [9, 10, 14, 13, 19]. However, the Birkhoff-Rott equation is still rather delicate: a more in depth treatment of its analytical properties will be given in Section 1.1.

Perhaps most striking manifestation of the delicate behavior of this equation can be seen by linearizing its evolution about the flat vortex sheet u_{KH}. We review the classical derivation of the linearized equation and the associated

instability in Section 2.1, but the outcome is that the strength of the instability grows linearly with the magnitude of the wavenumber. This instability is observed both numerically and experimentally, and is known as the Kelvin-Helmholtz instability. In those observations, the flat sheet generally evolves into some number of counter-rotating spiraling interfaces. The term *Kelvin-Helmholtz instability* is used by some authors to refer to the specific linear instability of the flat sheet, and by others to describe the tendency of vortex sheets to break down into spirals; when we refer to the Kelvin-Helmholtz instability we take the more inclusive meaning.

The strength of the linear instability is compelling both in attempting to describe the vortex roll up seen in practice as well as the loss of analyticity of vortex sheets observed in mathematical studies. However, this work seeks to illustrate ways in which the linearized instability analysis of the flat sheet may be overly simplistic. We posit that the global geometry of vortex sheets may significantly affect how instabilities are manifest.

In particular, we study the circular vortex sheet which corresponds to the steady velocity field

$$u_C(x,t) \equiv u_C(x) = \begin{cases} u^+ \frac{x^\perp}{|x|^2} & \text{for } |x| > R \\ u^- \frac{x^\perp}{|x|^2} & \text{for } |x| > R \end{cases},$$

where u^+, u^- are again scalars with $u^+ \neq u^-$. We remark that utilizing the Birkhoff-Rott formulation corresponds to the situation where $u^- = 0$, as otherwise there will be an implicit point vortex at the origin. The circular vortex sheet has physical relevance, including geometric similarity to spiraling fluid phenomena such as ocean eddies. It is also similar to the sharp shear layers observed in atmospheric systems, including hurricane eyewalls and storms on the surfaces of gas giants including Saturn [1, 2]. Unlike the latter cases, we study circular vortex sheets at a sufficiently small scale where the rotation of the planet does not provide a stabilizing effect.

It has previously been observed that circular vortex sheets still exhibit similar numerical instabilities as the flat vortex sheet [40]. As such, and since a circular sheet locally looks flat, one would anticipate that the linearized analysis of the circular sheet should be similar to that of the flat sheet. Our first main result, stated here informally, establishes that this is not the case.

Theorem 1.1 (Informal)**.** *The linearized Birkhoff-Rott equation is stable when centered on the steady circular sheet.*

This theorem stands in stark contrast with the flat sheet, demonstrating how geometry can have a crucial effect on how we should think about the Birkhoff-Rott equation. In particular, for the circular sheet it would be crucial to study non-linear effects in order to understand the instabilities: we delay such a study to future work. To our knowledge this is also the first example of a steady solution to the Birkhoff-Rott equation which is not linearly unstable, we give further discussion about this in Section 1.1.

On the other hand, numerical experiments still display unstable effects. Such experiments are necessarily based upon smooth approximations of the Birkhoff-Rott kernel. Our second main contribution derives a matrix representation (when considering a sine/cosine modes) of the linearized evolution equation for circular sheets under kernel regularized dynamics, and establishes conditions under which they are stable or unstable. As a particular case, we show that popular the kernel regularization introduced in [21] is linearly unstable for high-frequency perturbations. Summarized here, this result stands in contrast with the flat Kelvin-Helmholtz instability, where regularization is known to decrease the instability across high wavenumbers, and highlights the challenge of constructing numerical schemes for the Birkhoff-Rott equation.

Proposition 1.1 (Informal)**.** *The Krasny regularization of the generalized Birkhoff-Rott kernel is linearly unstable under high-frequency perturbations of the steady circular sheet.*

We now outline the remainder of this work. Section 1.1 provides a more detailed accounting of previous work in this area, including analytical, numerical, and experimental results for vortex sheets. In Section 2 we review the classical linearized analysis for the Kelvin-Helmholtz instability, and then demonstrate how the analysis changes for the circular sheet, culminating in Theorem 2.1 (a more precise version of Theorem 1.1). In Section 3 we study the problem of linear stability for more general kernels, including those utilized in both numerics and analysis. We derive a characterization of stability, with the condition for linear stability given in Proposition 3.1 and the condition for linear instability given in Proposition 3.2. Next we prove Proposition 3.3, which is a more precise statement of Proposition 1.1 and indicates that the Krasny kernel [21] is unstable under high-frequency perturbations. In Section 4 we review standard numerical methods utilized in studying vortex sheet dynamics and illustrate the instabilities observed numerically, as previously recorded in [40]. Finally, in Section 5 we show experiments used to illustrate the instability of the circular vortex sheet. The experimental setup that we use builds upon earlier works studying the stability of storm patterns on Saturn, but our focus is upon how the circular shear layer destabilizes upon removal of stabilizing centrifugal forces. The experiments give an excellent qualitative match of the shapes that we observe numerically, see Figures 7 and 8, which suggests that even though the numerics do not match the analytical stability of the classical Birkhoff-Rott equation, they still may provide predictive utility.

1.1 Related Work

The evolution of vortex sheets has been widely studied in the mathematical literature. The derivations and an in-depth account of many analytical properties of the Birkhoff-Rott equation can be found in the classical book [28], as well as in the introduction of [42].

It is well-known that the Birkhoff-Rott equation is rather delicate, and is ill-posed in the sense of Hadamaard (in appropriate C^k or H^s spaces) [8, 12].

Indeed, one can show that, for closed vortex sheets, if a solution is $C^{1+\rho}$ then it must also be C^∞ [25]. On the positive side, by a Cauchy-Kowalevski type argument, it is known [25] that if a curve is initially analytic then there exists a solution to the Birkhoff-Rott equation for short time. Conditions establishing the equivalence between solutions of Birkhoff-Rott and a weak version of Euler's equation is given in [27]. The connection between solutions of the incompressible Euler equation with vortex sheet initial data and smoothed approximations of the same have also been studied by a number of authors, see e.g. [26, 27].

The Kelvin-Helmholtz instability was first studied in the late 19th century. The modern approach and derivation, which has an elegant connection with Fourier analysis and Hilbert transforms, appeared in [12] and is clearly presented in Chapter 9 of [28]. Many of the early works about well- and ill-posedness centered on perturbations of the flat sheet. This was partially driven by a number of classic numerical studies which provided evidence for spiral roll up from flat sheets [22, 31]. Experimental observation of the instability and subsequent roll-up of the flat sheet were also well-known at the time, see e.g. the classic book [11]. This type of spiral roll-up is expected to be self-similar, and a wide range of numerical and analytical work has sought to better understand self-similar solutions to Euler's equation which resemble vortex sheets [7, 14, 15, 36, 37, 9, 10].

Numerical methods for vortex sheets require delicate attention, especially in regions where the sheet nearly self-intersects: this can be immediately seen by noticing that the need for a principal value integral in the definition of the Birkhoff-Rott equation. Important classical works regarding numerical approximation of vortex sheets include [23, 33]. Often these methods boil down to discretizing the vortex sheet into point vortices and solving for their evolution with out of the box Runge-Kutta methods. For many classical examples of incompressible vortex sheet evolution, including the Kelvin-Helmholtz instability, it is necessary to replace the singular kernel with a regularized approximation. An excellent overview of this process is presented by [24]. The regularization approach also connects directly with other non-local and kernel-driven evolution equations, such as the α-Euler equations and aggregation equations: these have also been generalized to vortex sheet evolution and studied analytically and numerically in [3, 40]. These works motivate our study of the generalized Birkhoff-Rott equation in Section 3, and there we give explicit formulas for kernels used in the above sources. We also note that forward in time analytical properties of motion driven by these regularized kernels tend to be much better than those of the standard Birkhoff-Rott equation, see, e.g. [4].

There are two important references which pertain specifically to circular vortex sheets, and which provide a backdrop for our work. The classical work [29] demonstrates the instability of a circular shear interface with respect to **velocity** perturbations: that is they study the stability of solutions to Euler's equation perturbing off of the velocity profile given by a circular shear flow. This aligns with the intuition that the reduction to the Birhkoff-Rott equation should remove certain classes of instabilities. Our work directly studies the stability problem with respect to **geometric** perturbations in the context of Birkhoff-Rott, thus respecting the structure that vorticities are supported on

a curve, and within this class we obtain a stability result that contrasts with theirs. More recently, [40] numerically studied the (in)stability of circular vortex sheets for a variety of kernels, including the standard Birkhoff-Rott kernel as well as kernels from aggregation equations. In their work they discuss analytical characterization of the linear instability as desirable, but to our knowledge subsequent research in that direction was focused only on the case of gradient type kernels from aggregation equations [20].

Outside of the infinite flat and closed circular sheet there are relatively few explicit solutions to the Birkhoff-Rott equation. Two notable examples are limits of the rotating Kirchhkoff ellipse (described, e.g. in [5]) and the Prandtl-Munk vortex [32]. These can be used as building blocks for other families of vortex sheets [34]. The instability of these solutions was recently studied in [35]: in that case the instability can be rather weak, corresponding to algebraic growth. In their work they study only perturbations of the vortex sheet itself, as opposed to perturbations of the underlying velocity fields as in [29]: we follow the same methodology. Their conclusion is that, for the limit of Kirchhoff ellipses and for the Prandtl-Munk vortices that the instability grows stronger in the wavenumber, and hence is similar in character to the flat sheet Kelvin-Helmholtz instability, a phenomenon that we do not observe in our case.

Other studies of circular vortex sheets have appeared in the physics and experimental literature. Some of this work is inspired by the observation of a stable hexagonal structure on the north polar surface of Saturn, composed of clouds in relative motion. This structure has persisted without any significant changes since it was first observed by the Voyager spacecraft in 1988 [2, 17]. Since the structure is essentially a perturbed circular shear layer, this physical example is highly relevant to our work.

The hexagon has been studied directly in [1], where the authors postulate that it emerged and persists by the equilibration of vertically uniform jets and shear layers. Such equilibration in the context of Saturn can be attributed to relative rotation of the hexagonal structure with respect to the background rotation of the planet. The study [1] strongly relies upon the earlier work [16], which also experimentally demonstrates the steady equilibriation of polygonal vortex patterns on a shear layer in a rotating fluid.

An early experimental work attempted to eliminate centrifugal and Coriolis forces to observe what the authors refer to as the Kelvin-Helmholtz instability on a circular shear layer [38]. However, since the authors chose to maintain a forcing background rotation and used a very small fluid depth, they produced steady polygonal patterns of vortices very much like the later studies [1, 16]; the dynamics observed were not that of Kelvin-Helmholtz instability. These difficulties are discussed further in the experimental section of this paper. In our experimental study we use a similar test setup, but make modifications to the procedure to ensure the observed dynamics isolate the development of the instability.

2 Linearized Analysis of the Birkhoff-Rott Equation

In this section, we conduct a linearized analysis of specific vortex sheet solutions to the classical Birkhoff-Rott equation, namely

$$\partial_t z^*(\alpha,t) = \frac{1}{2\pi i}\text{P.V.}\int \frac{1}{z(\alpha,t)-z(\beta,t)}\,d\beta.$$

We begin by reviewing the classical analysis for the flat vortex sheet, and then turn our attention to the circular sheet.

2.1 Kelvin-Helmholtz Instability on Flat Vortex Sheets

In reviewing the linearized theory for the Birkhoff-Rott equation near flat vortex sheets our description will follows the classical exposition given in [28]. While this theory is largely classical, it offers an important starting point when we examine the circular vortex sheet in the next subsection. We begin by considering the perturbation of the flat sheet $z : (-\infty,\infty)\times[t_0,t_1]\to\mathbb{C}\sim\mathbb{R}^2$ described by $z(\alpha,t)=\alpha+\xi(\alpha,t)$, where ξ is uniformly smooth and small in $\mathbb{C}$. For $\xi\equiv 0$ we have a constant solution to the classical Birkhoff-Rott Equation (1.2). For a nonzero perturbation we obtain

$$\begin{aligned}\partial_t z^*(\alpha,t)=\partial_t\xi^*(\alpha,t) &= \frac{1}{2\pi i}\text{P.V.}\int_{\mathbb{R}}\frac{1}{\alpha+\xi(\alpha)-\beta-\xi(\beta)}d\beta\\ &= \frac{1}{2\pi i}\text{P.V.}\int_{\mathbb{R}}\frac{1}{\alpha-\beta}\frac{1}{1+\mathcal{E}}d\beta,\end{aligned}$$

where

$$\mathcal{E}=\frac{\xi(\alpha)-\xi(\beta)}{\alpha-\beta}.$$

Because ξ is uniformly small and smooth, so is its spatial derivative $\partial_\alpha\xi$. The quantity $\mathcal{E}$ approximates the difference quotient when β approaches α, so it is small as well. Therefore, we linearize about $\mathcal{E}=0$ to obtain

$$\frac{1}{2\pi i}\text{P.V.}\int_{\mathbb{R}}\left(\frac{1}{\alpha-\beta}-\frac{\xi(\alpha)-\xi(\beta)}{(\alpha-\beta)^2}\right)d\beta.$$

Using the fact that

$$\text{P.V.}\int_{\mathbb{R}}\frac{1}{\beta}d\beta=0$$

and applying integration by parts on the second term, we obtain

$$\partial_t\xi^*(\alpha,t)=\frac{1}{2}\mathcal{H}\partial_\alpha\xi(\alpha,t), \tag{2.1}$$

where $\mathcal{H}$ is the Hilbert transform

$$\mathcal{H}f(x)=\frac{1}{\pi i}\int_{\mathbb{R}}\frac{f(y)}{y-x}dy.$$

If we write ξ as the Fourier mode

$$\xi(\alpha,t) = A_k(t)e^{ik\alpha} + B_k(t)e^{-ik\alpha},\ k>0,$$

then the Hilbert transform of $\partial_\alpha \xi$ is given by

$$\mathcal{H}\partial_\alpha \xi(\alpha,t) = ikA_k(t)e^{ik\alpha} + ikB_k(t)e^{-ik\alpha}.$$

For an introduction of the Hilbert transform in the context of this problem, see [28]. This transform is then used to solve the linearized Equation (2.1), yielding expressions for the kth Fourier coefficients

$$\begin{aligned} A_k(t) &= A_k^+ e^{kt/2} + A_k^- e^{-kt/2}, \\ B_k(t) &= B_k^+ e^{kt/2} + A_k^- e^{-kt/2}, \end{aligned}$$

where $A_k^+ = -iB_k^{+*}$ and $A_k^- = iB_k^{-*}$. We see here that a component of the kth Fourier mode grows exponentially as $e^{|k|t/2}$, implying that the linear evolution problem is highly unstable. Indeed, the instability grows in wavenumber, a fact that some authors describe as a common theme of instability of vortex sheets [35]. The authors of [28] go on to show that there is a family of initially analytic solutions to Equation (2.1) which develop a singularity in finite time.

2.2 Linearized Stability for Circular Vortex Sheets

We now consider the evolution of a circular vortex sheet $z : [0,2\pi]\times[t_0,t_1] \to \mathbb{C}\sim\mathbb{R}^2$ described by $z(\alpha,t) = e^{i(\alpha+t/2)}$ for $\alpha\in[0,2\pi]$. As for the planar Kelvin-Helmholtz instability, our starting point is the classical Birkhoff-Rott Equation 3.1. To verify that z is a solution, we compute

$$\begin{aligned} \partial_t z^*(\alpha,t) &= \frac{1}{2\pi i}\text{P.V.}\int_0^{2\pi} \frac{1}{z(\alpha,t)-z(\beta,t)}d\beta \\ &= \frac{e^{-i(\alpha+Ct)}}{2\pi i}\text{P.V.}\int_0^{2\pi}\frac{1}{1-e^{i(\beta-\alpha)}}d\beta. \end{aligned}$$

In order to simplify our expressions, we will utilize the following generalized formula for the principal value of the Cauchy integral [6, 18].

Lemma 1 (Cauchy integral formula for Jordan curves)**.** *Let Γ be a rectifiable, closed, positively oriented Jordan curve in $\mathbb{C}$ which defines the interior region Ω^- and exterior region Ω^+. Let $f:\Gamma\to\mathbb{C}$ be an analytic function and $w_0\in\mathbb{C}/\Gamma$. The well-known Cauchy integral formula states*

$$\frac{1}{2\pi i}P.V.\int_\Gamma \frac{f(w)}{w-w_0}dw = \begin{cases} f(w_0) & \text{for } w_0\in\Omega^- \\ 0 & \text{for } w_0\in\Omega^+ \end{cases}.$$

Now suppose $w_0\in\Gamma$; then the Cauchy integral of f at w_0 takes the principal value

$$\frac{1}{2\pi i}P.V.\int_\Gamma \frac{f(w)}{w-w_0}dw = \frac{f(w_0)}{2}.$$

Continuing our computation from above, after changing variables to the unit circle (oriented counterclockwise) with the relation $w = e^{i(\beta-\alpha)}$ we obtain by Lemma 1

$$\begin{aligned}
&\frac{-e^{-i(\alpha+Ct)}}{2\pi}\text{P.V.}\int_{\partial B}\frac{1}{w(1-w)}dw \\
&= \frac{-e^{-i(\alpha+Ct)}}{2\pi}\text{P.V.}\int_{\partial B}\frac{1}{w}-\frac{1}{w-1}dz \\
&= -i/2e^{-i(\alpha+Ct)}.
\end{aligned}$$

For this initial condition the left hand side of the Birkhoff-Rott equation is

$$\partial_t z^*(\alpha,t) = -iCe^{-i(\alpha+Ct)},$$

implying that for $C = 1/2$ the circle is a solution to the Birkhoff-Rott equation. This solution z takes the form of a traveling wave corresponding to a steady vorticity distribution; this stands in contrast with the infinite flat sheet studied for the classical Kelvin-Helmholtz instability in which points on the steady sheet do not move.

To examine the linear stability of this solution, we begin by considering the a smooth, 2π-periodic perturbation $\xi(\alpha,t)$ where $||\xi||_{C^2} \ll 1$. The perturbed circular vortex sheet is then defined by $z(\alpha,t) = e^{i(\alpha+t/2)}(1+\xi(\alpha,t))$. We then rewrite the right hand side of the Birkhoff-Rott equation as

$$\begin{aligned}
\partial_t z^*(\alpha,t) &= \frac{1}{2\pi i}\text{P.V.}\int\frac{1}{z(\alpha,t)-z(\beta,t)}d\beta \\
&= \frac{e^{-i(\alpha+t/2)}}{2\pi i}\text{P.V.}\int\frac{1}{1+\xi(\alpha)-e^{i(\beta-\alpha)}(1+\xi(\beta))}d\beta \\
&= \frac{e^{-i(\alpha+t/2)}}{2\pi i}\text{P.V.}\int\frac{1}{1-e^{i(\beta-\alpha)}}\frac{1}{1+\mathcal{E}}d\beta,
\end{aligned}$$

where $\mathcal{E}$ is the small quantity

$$\mathcal{E} = \frac{\xi(\alpha)-e^{i(\beta-\alpha)}\xi(\beta)}{1-e^{i(\beta-\alpha)}}.$$

The smallness of $\mathcal{E}$ follows from the assumption that $||\xi||_{C^2} \ll 1$. Taylor expanding about $\mathcal{E} = 0$ to first order, we obtain

$$\partial_t(e^{i(\alpha+t/2)}(1+\xi(\alpha,t)))^* \approx \frac{e^{-i(\alpha+t/2)}}{2\pi i}\text{P.V.}\int\frac{1}{1-e^{i(\beta-\alpha)}}-\frac{\xi(\alpha)-e^{i(\beta-\alpha)}\xi(\beta)}{(1-e^{i(\beta-\alpha)})^2}d\beta$$

which implies that the perturbation ξ evolves by

$$\partial_t(e^{i(\alpha+t/2)}\xi(\alpha,t))^* \approx \frac{-e^{-i(\alpha+t/2)}}{2\pi i}\text{P.V.}\int\frac{\xi(\alpha)-e^{i(\beta-\alpha)}\xi(\beta)}{(1-e^{i(\beta-\alpha)})^2}d\beta. \tag{2.2}$$

We change variables by $w = e^{i(\beta-\alpha)}$, and let $\tilde{\xi}(w) = \xi(\beta)$ so that $\tilde{\xi}(1) = \xi(\alpha)$. The right hand side then becomes

$$\frac{e^{-i(\alpha+t/2)}}{2\pi}\text{P.V.}\int_{\partial B}\frac{\tilde{\xi}(1)-w\tilde{\xi}(w)}{w(1-w)^2}dw \tag{2.3}$$

$$=\frac{e^{-i(\alpha+t/2)}}{2\pi}\text{P.V.}\int_{\partial B}(\tilde{\xi}(1)-w\tilde{\xi}(w))\left(\frac{1}{w}-\frac{1}{w-1}+\frac{1}{(w-1)^2}\right)dw. \tag{2.4}$$

For ease of manipulating the Cauchy integral operators, we will assume for now that ξ permits an analytic extension to the strip $[0, 2\pi] \times \mathbb{R}$, i.e. that $\xi((\ln w)/i + \alpha, t)$ is analytic in w. The Fourier modes e^{ikx} are an example of such a perturbation, and such functions are dense in many relevant function spaces, such as $L^2(\mathbb{S})$. Under this assumption we then have that $\tilde{\xi}(w)$ is analytic. For the first term in (2.4) we may then use the classical Cauchy integral formula (i.e. the first part of Lemma 1) to directly compute

$$\frac{e^{-i(\alpha+t/2)}}{2\pi}\text{P.V.}\int_{\partial B}\frac{\tilde{\xi}(1)-w\tilde{\xi}(w)}{w}dw = ie^{-i(\alpha+t/2)}\tilde{\xi}(1) = ie^{-i(\alpha+t/2)}\xi(\alpha).$$

For the second and third terms in (2.4) we Taylor expand the numerator $\tilde{\xi}(1) - w\tilde{\xi}(w)$ about $w = 1$ as

$$\tilde{\xi}(1)-w\tilde{\xi}(w) = (-\tilde{\xi}'(1)-\tilde{\xi}(1))(w-1)+R_1(w)(w-1)^2,$$

where the remainder $R_1(w)$ is analytic. Substituting this Taylor expansion into the remaining terms of (2.4) yields

$$\frac{e^{-i(\alpha+t/2)}}{2\pi}\text{P.V.}\int_{\partial B}(\tilde{\xi}'(1)+\tilde{\xi}(1))(1-\frac{1}{(w-1)})+R_1(w)(1-(w-1))\,dw.$$

The classical Cauchy integral formula cancels the first, third, and fourth of these terms. Utilizing Lemma 1 then returns

$$\begin{aligned}\frac{e^{-i(\alpha+t/2)}}{2\pi}\text{P.V.}\int_{\partial B}\frac{-\tilde{\xi}'(1)-\tilde{\xi}(1)}{w-1}dw &= i/2e^{-i(\alpha+t/2)}(-\tilde{\xi}'(1)-\tilde{\xi}(1))\\ &= e^{-i(\alpha+t/2)}(-1/2\partial_\alpha\xi(\alpha)-i/2\xi(\alpha)).\end{aligned}$$

Returning to (2.2), after taking the derivatives of the left hand side and collecting terms we obtain

$$e^{-i(\alpha+t/2)}(-i/2\xi^*(\alpha,t)+\partial_t\xi^*(\alpha,t)) = e^{-i(\alpha+t/2)}(i\xi(\alpha,t)-i/2\xi(\alpha,t)-1/2\partial_\alpha\xi(\alpha,t))$$

which simplifies to the partial differential equation

$$\partial_t\xi^*(\alpha,t) = i/2(\xi(\alpha,t)+\xi^*(\alpha,t))-1/2\partial_\alpha\xi(\alpha,t)$$

or equivalently,

$$\partial_t\xi^*(\alpha,t) = iRe(\xi(\alpha,t))-1/2\partial_\alpha\xi(\alpha,t). \tag{2.5}$$

Although we assumed that ξ admitted a certain analytic extension in manipulating the Cauchy integrals, this linearized equation makes sense for a wide class of perturbations. Indeed, as all of the manipulations were justified for the standard Fourier basis, we can treat this expression as equivalent within the space of L^2 perturbations.

This equation admits a closed form solution by the method of characteristics. Writing the perturbation as a sum of real and imaginary parts $\xi = \xi_R + i\xi_I$, Equation (2.5) becomes

$$\partial_t(\xi_R(\alpha,t) - i\xi_I(\alpha,t)) = i\xi_R(\alpha,t) - \frac{1}{2}\partial_\alpha(\xi_R(\alpha,t) + i\xi_I(\alpha,t)).$$

Splitting the previous equation into real and imaginary parts yields

$$\begin{aligned}
&\partial_t\xi_R + 1/2\partial_\alpha\xi_R = 0,\\
&-\partial_t\xi_I(\alpha,t) - \xi_R(\alpha,t) + \frac{1}{2}\partial_\alpha\xi_I(\alpha,t) = 0.
\end{aligned}$$

First consider the real part $\partial_t\xi_R + 1/2\partial_\alpha\xi_R = 0$. By the method of characteristics we obtain

$$\xi_R(\alpha,t) = f_1(\alpha - t/2),$$

where $f_1(\alpha_0)$ is the real initial data as a function of the spatial coordinate. The characteristics for the real part are $t(s) = s$ and $\alpha(s) = s/2 + \alpha_0$. For the imaginary part $-\partial_t\xi_I(\alpha,t) - \xi_R(\alpha,t) + \frac{1}{2}\partial_\alpha\xi_I(\alpha,t) = 0$ we use the method of characteristics to obtain

$$\xi_I(\alpha,t) = f_2(\alpha + t/2) + \int_0^t f_1(\alpha - w/2)dw,$$

where $f_2(\alpha_0)$ is the imaginary initial data as a function of the spatial coordinate. The imaginary part has characteristic curves $t(s) = -s$ and $\alpha(s) = s/2 + \alpha_0$. Note that although the characteristic directions in time are different, we can still solve Equation (2.5) because the real part is decoupled. The combination of real and imaginary parts gives the closed-form solution

$$\begin{aligned}
&\xi_R(\alpha,t) = f_1(\alpha - t/2),\\
&\xi_I(\alpha,t) = f_2(\alpha + t/2) + \int_0^t f_1(\alpha - w/2)dw,
\end{aligned} \tag{2.6}$$

where f_1, f_2 are arbitrary initial data.

We notice that as long as f_1 has mean zero, then both ξ_R, ξ_I remain bounded, in the sense that $\|\xi_R(\cdot,t)\|_2 < C\|\xi(\cdot,0)\|_2, \|\xi_I(\cdot,t)\|_2 < C\|\xi(\cdot,0)\|_2$, with C independent of t and ξ. We also notice that the same bounds are true in L^∞. If f_1 has non-zero mean then we can re-center our solution about another steady state (i.e. a circle with slightly bigger radius).

Hence we have proved the following:

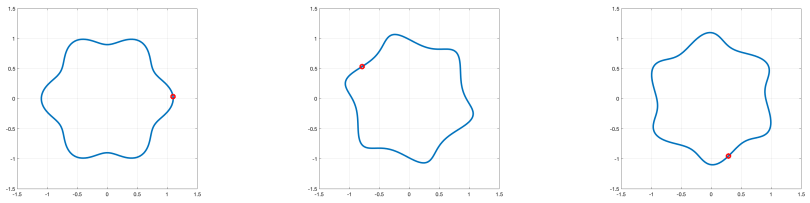

(a) $t = 0$ (b) $t = 5$ (c) $t = 10$

Figure 1: Stable evolution of the linearized problem.

Theorem 2.1. *When centered about the circular vortex sheet, the linearized Birkhoff-Rott equation can be written as a complex-valued transport equation on the circle, namely Equation* (2.5)*. This equation admits an explicit solution formula* (2.6)*, and assuming the original equation is appropriately centered (i.e. the perturbations have average real part of zero) then this solution map is uniformly stable in either* L^2 *or* L^∞*.*

This theorem mirrors the simplicity of the Hilbert transform and the solution formula via Fourier series in the previous section, but with a completely different result: that perturbations of the circular sheet are uniformly stable. They are, in essence, governed by a slight modification of the wave equation, and the type of uniform stability that we observe for the wave equation also is manifest here. This is striking for many reasons. First, the delicate ill-posedness behavior of the original Birkhoff-Rott equation disappears at the linear level. This means that the most important terms for describing sheet breakdown and singularity formation in this case must be non-linear! Furthermore, to our knowledge this is the first known example of a vortex sheet which is even linearly stable (within the class of perturbations of the sheet itself, as opposed to velocity perturbations).

As an example, the real cosine perturbation initially defined by $f_1(\alpha) = a\cos k\alpha,\ f_2(\alpha) = 0$ yields the stable travelling wave solution

$$\xi(\alpha, t) = a\cos(k(\alpha - t/2)) + i\frac{2a}{k}\left(\sin(k\alpha) - \sin(k(\alpha - t/2))\right).$$

Figure 1 plots the travelling wave solution given by the combination of the steady solution with (2.6) for the initial condition $f_1(\alpha) = 0.1\cos 6\alpha,\ f_2(\alpha) = 0$. The overall rotation of the vortex sheet can be seen by the red tracking point. The wave travels around the steady solution and its shape fluctuates slightly, but it remains stable.

Remark 2.2. *It is also possible to evaluate the stability of the linear evolution problem by writing the perturbation as*

$$\xi(\alpha, t) = (a_k(t) + ib_k(t))\cos(k\alpha) + (c_k(t) + id_k(t))\sin(k\alpha),$$

where $k \in \mathbb{N}$ and a_k, b_k, c_k, and d_k are real Fourier coefficients. We can then write (2.5) *as*

$$\frac{d}{dt}\begin{bmatrix} a_k \\ b_k \\ c_k \\ d_k \end{bmatrix} = \begin{bmatrix} 0 & 0 & -k/2 & 0 \\ -1 & 0 & 0 & k/2 \\ k/2 & 0 & 0 & 0 \\ 0 & -k/2 & -1 & 0 \end{bmatrix} \begin{bmatrix} a_k \\ b_k \\ c_k \\ d_k \end{bmatrix}.$$

The eigenvalues associated with this system are $\lambda = \pm ik/2$ each with geometric multiplicity of two. The matrix can be completely diagonalized about these eigenvalues, thereby implying stable oscillation of the perturbation about the circular vortex sheet. This approach mirrors that of the Kelvin-Helmholtz instability on a flat sheet, but the solution via characteristics provides more direct insight.

Finally, it is tempting to think that the flat sheet should be attainable as a limit of infinitely large circular sheets. We notice that this is not the case for at least one clear reason: the principal value in the flat sheet must accommodate cancellations at spatial infinity that are not present in the circular sheet. Furthermore, the circular sheet also does add an additional implicit constraint that the velocities on the interior of the shear interface are zero: otherwise the there is an implicit vortex point at the origin. This type of constraint is not relevant in the case of the flat sheet, as one can add a globally constant flow in the direction of the interface to attain any desired velocity without changing the strength of the vortex sheet.

3 Generalized Birkhoff-Rott

The explicit formulas in the previous section are compelling, but do not correspond to the previously observed instability of circular sheets in numerical simulations [40]. Of course such instability could be solely a non-linear effect, but in our experience this instability is rather robust in simulation: hence in this section we examine the stability of the circular sheet under a more general class of models including those which are commonly used in numerical simulations (and in other analytical studies).

In particular, we will consider a class of generalized Birkhoff-Rott equations which use a regularizing kernel to avoid the singularity of the classical Birkhoff-Rott equation. We will consider curve evolution equations of the form

$$\partial_t z^*(\alpha, t) = \frac{1}{2\pi i}\text{P.V.} \int K(z(\alpha, t), z(\beta, t))\, d\beta, \tag{3.1}$$

where the kernel K can be written as

$$K(z_1, z_2) = \frac{(z_1 - z_2)^*}{f(|z_1 - z_2|)}, \tag{3.2}$$

where f is a real-valued, non-negative function. The assumption that the kernel have $z_1^* - z_2^*$ in the numerator guarantees that the velocity field is purely

rotational (i.e. incompressible), and the fact that f only depends upon the distance between z_1, z_2 relates to a type of isotropy of the velocities induced by the "vorticity". Kernels of this form include the following:

- When $K(z_1, z_2) = \frac{1}{z_1 - z_2}$ we have that $f(|z_1 - z_2|) = |z_1 - z_2|^2$, and then Equation (3.1) corresponds to the classical Birkhoff-Rott equation.
- When $K(z_1, z_2) = \frac{(z_1 - z_2)^*}{|z_1 - z_2|^2 + \delta^2}$ for some $\delta > 0$ then Equation (3.1) corresponds to the popular regularized numerical methods proposed by [21]. These are also the kernels reported in [40].
- When $K(z_1, z_2) = \frac{1}{z_1 - z_2}\left(1 - \frac{|z_1 - z_2|}{\alpha} K_1\left(\frac{|z_1 - z_2|}{\alpha}\right)\right)$, where K_1 is a modified Bessel function, then this corresponds to the α-Birkhoff-Rott equation proposed in [4]. This equation can also be obtained by replacing the Biot-Savart law $\nabla^\perp \Delta^{-1}\omega = v$ with $(I - \delta^2\Delta)^{-1}\nabla^\perp \Delta^{-1}\omega = v$, see Section 2 in [4] for details.
- One could also consider power-law forms of Birkhoff-Rott where $K(z_1, z_2) = \frac{(z_1 - z_2)^*}{|z_1 + z_2|^{2-\delta}}$, with $\delta > 0$.

Each of these essentially corresponds to a different choice of kernel in the Biot-Savart law. Here we restrict our attention to purely incompressible flows: this rules out the aggregation type kernels previously considered in [40].

3.1 Linearized Instability for Circular Vortex Sheets Under General Kernels

We now consider the linear evolution problem for a circular vortex sheet under general kernels which are of the form (3.2). For analytical convenience, and motivated by the kernels used in practice, we will make the additional assumption that $f : (0, 3) \to (0, \infty)$ is a C^1 function satisfying, for some $\kappa > 1/2$,

$$\lim_{y \to 0} \frac{1}{y^\kappa} \int_0^y \left| \frac{1}{f(z)} \right| dz < \infty, \qquad \lim_{y \to 0} \frac{1}{y^\kappa} \int_0^y \left| \frac{z f'(z)}{f^2(z)} \right| dz < \infty. \tag{3.3}$$

We notice that if f is uniformly bounded away from zero then we may take $\kappa = 1$. We also notice that since $f \in C^1$ and maps into $(0, \infty)$ the the previous assumption also implies integrability of both $\frac{1}{f}$ and $\frac{z f'}{f^2}$ on $(0, 3)$. Finally, we mention that the domain $(0, 3)$ is for convenience, since the input of f, f' is always $|e^{i\alpha} - e^{i\beta}|$, which takes values between 0 and 2.

Under these assumptions, we may write the generalized Birkhoff-Rott Equation (3.1) as

$$\partial_t z^*(\alpha, t) = \frac{1}{2\pi i} \int \frac{z^*(\alpha) - z^*(\beta)}{f(|z(\alpha) - z(\beta)|)} d\beta,$$

where we may safely remove the principal value since the integrals are now finite. We note that by making the assumption (3.3) we have ruled out the classical

Birkhoff-Rott case, but still permit the kernels used in [23] and [4], as the former is strictly bounded away from zero and the latter only has logarithmic growth near zero.

As in our analysis of the classical Birkhoff-Rott equation in the previous subsection, we consider the evolution of the perturbed circular vortex sheet described by $z(\alpha,t) = e^{i(\alpha+Ct)}(1+\xi(\alpha))$ for $\alpha \in [0,2\pi]$ and some constant C (with a value given below). Equation (3.1) then becomes

$$\partial_t(e^{i(\alpha+Ct)}(1+\xi(\alpha))) = \frac{-e^{iCt}}{2\pi i}\int_0^{2\pi} \frac{e^{i\alpha}(1+\xi(\alpha)) - e^{i\beta}(1+\xi(\beta))}{f(|e^{i\alpha}(1+\xi(\alpha)) - e^{i\beta}(1+\xi(\beta))|)}d\beta.$$

Assuming that ξ is small, we Taylor expand the integrand about the steady solution ($\xi \equiv 0$) to obtain

$$\begin{aligned}\partial_t(e^{i(\alpha+Ct)}(1+\xi(\alpha))) \approx \frac{-e^{iCt}}{2\pi i}\int_0^{2\pi} &\frac{e^{i\alpha}-e^{i\beta}}{f(|e^{i\alpha}-e^{i\beta}|)} + \frac{e^{i\alpha}\xi(\alpha) - e^{i\beta}\xi(\beta)}{f(|e^{i\alpha}-e^{i\beta}|)} \\ &- \frac{f'(|e^{i\alpha}-e^{i\beta}|)(e^{i\alpha}-e^{i\beta})Re((e^{i\alpha}\xi(\alpha) - e^{i\beta}\xi(\beta))(e^{-i\alpha}-e^{-i\beta}))}{f(|e^{i\alpha}-e^{i\beta}|)^2|e^{i\alpha}-e^{i\beta}|}\,d\beta.\end{aligned}$$

Here we notice that in the second term for the chain rule we needed to use the fact that the derivative of $|\cdot|$ at a point z in the direction w is written in complex variables as $\frac{Re(z^*w)}{|z|}$, as can readily be verified by rewriting the complex numbers as vectors in $\mathbb{R}^2$.

The first term corresponds to the steady case where $\xi \equiv 0$, i.e.

$$\partial_t e^{i(\alpha+Ct)} = iCe^{i(\alpha+Ct)} = \frac{-e^{i(\alpha+Ct)}}{2\pi i}\int_0^{2\pi}\frac{1-e^{i(\beta-\alpha)}}{f(|e^{i\alpha}-e^{i\beta}|)}d\beta.$$

This gives us a formula for C (which is well-defined by Assumption (3.3)), namely

$$C = \frac{1}{2\pi}\int_0^{2\pi}\frac{1-e^{i(\beta-\alpha)}}{f(|e^{i\alpha}-e^{i\beta}|)}d\beta = \frac{1}{2\pi}\int_0^{2\pi}\frac{1-\cos(\tilde{\beta})}{f(|1-e^{i\tilde{\beta}}|)}\,d\tilde{\beta} \in \mathbb{R},$$

where we have used the oddness of sine and the 2π-periodicity of the argument of f. Returning to our computation, we see that the linearized equation is given by

$$\begin{aligned}\partial_t\xi(\alpha,t) = -iC\xi(\alpha) &- \frac{1}{2\pi i}\int_0^{2\pi}\frac{\xi(\alpha)-e^{i(\beta-\alpha)}\xi(\beta)}{f}\,d\beta \\ &+ \frac{1}{2\pi i}\int_0^{2\pi}\frac{f'}{f^2}\frac{(1-e^{i(\beta-\alpha)})Re((\xi(\alpha)-e^{i(\beta-\alpha)}\xi(\beta))(1-e^{-i(\beta-\alpha)}))}{|e^{i\alpha}-e^{i\beta}|}\,d\beta,\end{aligned}$$

where the argument of f and f' is $|e^{i\alpha}-e^{i\beta}|$ (which we omit for brevity). We notice that, again using the change of variables $\tilde{\beta} = \beta - \alpha$ and the oddness of

sine, we may simplify this somewhat to obtain

$$\begin{aligned}\partial_t \xi(\alpha,t) &= iM_1\xi(\alpha) + iM_2 Re(\xi(\alpha)) + M_3 Im(\xi(\alpha)) \\ &+ \frac{1}{2\pi i}\int_0^{2\pi} \frac{e^{i(\tilde{\beta})}\xi(\tilde{\beta}+\alpha)}{f(|1-e^{i\tilde{\beta}}|)}\,d\tilde{\beta} \\ &- \frac{1}{2\pi i}\int_0^{2\pi} \frac{f'(|1-e^{i\tilde{\beta}}|)(1-e^{i\tilde{\beta}})Re((e^{i\tilde{\beta}}\xi(\tilde{\beta}+\alpha))(1-e^{-i\tilde{\beta}}))}{f(|1-e^{i\tilde{\beta}}|)^2|1-e^{i\tilde{\beta}}|}\,d\tilde{\beta},\end{aligned}$$

with

$$\begin{aligned}M_1 &= \frac{1}{2\pi}\int_0^{2\pi} \frac{1}{f(|1-e^{i\tilde{\beta}}|)}d\beta - C = \frac{1}{2\pi}\int_0^{2\pi} \frac{\cos(\tilde{\beta})}{f(|1-e^{i\tilde{\beta}}|)}\,d\tilde{\beta} \\ M_2 &= -\frac{1}{2\pi}\int_0^{2\pi} \frac{f'(|1-e^{i\tilde{\beta}}|)(1-\cos(\tilde{\beta}))^2}{f(|1-e^{i\tilde{\beta}}|)^2|1-e^{i\tilde{\beta}}|}\,d\tilde{\beta} \\ M_3 &= \frac{1}{2\pi}\int_0^{2\pi} \frac{f'(|1-e^{i\tilde{\beta}}|)\sin^2(\tilde{\beta}))}{f(|1-e^{i\tilde{\beta}}|)^2|1-e^{i\tilde{\beta}}|}\,d\tilde{\beta}.\end{aligned}$$

We now suppose that

$$\xi(\alpha,t) = (a_k(t) + ib_k(t))\cos(k\alpha) + (c_k(t) + id_k(t))\sin(k\alpha), \tag{3.4}$$

where $k \in \mathbb{N}$ and a_k, b_k, c_k, and d_k are real Fourier coefficients. We use a sine/cosine series instead of complex exponentials due to the presence of the real part in the formula. After expanding using trigonometric identities, we can rewrite the linearized equation as the following system

$$\frac{d}{dt}\begin{bmatrix} a_k \\ b_k \\ c_k \\ d_k \end{bmatrix} = \begin{bmatrix} S & cI_2 \\ -cI_2 & S \end{bmatrix}\begin{bmatrix} a_k \\ b_k \\ c_k \\ d_k \end{bmatrix} \tag{3.5}$$

where

$$S = \begin{bmatrix} 0 & -M_1 + M_3 + M_4 + M_5 \\ M_1 + M_2 - M_4 + M_6 & 0 \end{bmatrix} \tag{3.6}$$

with

$$\begin{aligned}M_4 &= \frac{1}{2\pi}\int_0^{2\pi} \frac{\cos(k\tilde{\beta})\cos(\tilde{\beta})}{f(|1-e^{i\tilde{\beta}}|)}\,d\tilde{\beta}, \\ M_5 &= -\frac{1}{2\pi}\int_0^{2\pi} \frac{f'(|1-e^{i\tilde{\beta}}|)\cos(k\tilde{\beta})\sin^2(\tilde{\beta})}{f(|1-e^{i\tilde{\beta}}|)^2|1-e^{i\tilde{\beta}}|}\,d\tilde{\beta}, \\ M_6 &= -\frac{1}{2\pi}\int_0^{2\pi} \frac{f'(|1-e^{i\tilde{\beta}}|)\cos(k\tilde{\beta})(1-\cos(\tilde{\beta}))^2}{f(|1-e^{i\tilde{\beta}}|)^2|1-e^{i\tilde{\beta}}|}\,d\tilde{\beta},\end{aligned}$$

and

$$c = \frac{1}{2\pi}\int_0^{2\pi} \frac{\sin(k\tilde{\beta})\sin(\tilde{\beta})}{f(|1-e^{i\tilde{\beta}}|)}\,d\tilde{\beta} \\ -\frac{1}{2\pi}\int_0^{2\pi} \frac{f'(|1-e^{i\tilde{\beta}}|)\sin(k\tilde{\beta})\sin(\tilde{\beta})(1-\cos(\tilde{\beta}))}{f(|1-e^{i\tilde{\beta}}|)^2}\,d\tilde{\beta}.$$

The matrix in (3.5) provides a tool with which we can test the linearized stability of a given regularizing kernel. To this end, we define the quantity $m_k := (-M_1 + M_3 + M_4 + M_5)(M_1 + M_2 - M_4 + M_6)$, where the constants M_i are defined above, for any $k \in \mathbb{N}$.

There is a useful relationship between the eigenvalues of S and those of the matrix in (3.5). The eigenvalues of S are easily computed as $\lambda_s = \pm\sqrt{m_k}$. If $m_k \neq 0$ we can then diagonalize S as

$$\hat{S} = \begin{bmatrix} \lambda_s^1 & 0 \\ 0 & \lambda_s^2 \end{bmatrix}.$$

By the block structure of the matrix in (3.5), we then compute

$$\det\begin{pmatrix} \hat{S}-\lambda I_2 & cI_2 \\ -cI_2 & \hat{S}-\lambda I_2 \end{pmatrix} = \det((\hat{S}-\lambda I_2)^2 + c^2 I_2) \\ = \det\begin{pmatrix} (\lambda_s^1-\lambda)^2 + c^2 & 0 \\ 0 & (\lambda_s^2-\lambda)^2 + c^2 \end{pmatrix},$$

which yields eigenvalues $\lambda = \pm\sqrt{m_k} \pm ic$. We first notice that if $m_k < 0$, then the eigenvalues of S are purely imaginary, and the eigenvalues of (3.5) are purely imaginary as well. If c is nonzero these eigenvalues are distinct, and if c is equal to zero then the blocks of S are completely decoupled so the larger matrix can be fully diagonalized. Whether or not $c = 0$, we have stability of the system (3.5) and therefore for the linearized evolution problem of the generalized Birkhoff-Rott Equation (3.1). In this first case (i.e. $m_k < 0$, uniformly in k), the change of variables which diagonalizes the system matrix in (3.5) will be uniformly invertible. As the sine and cosine series provides an orthonormal basis of L^2, this implies that in this case there exists a norm which is equivalent to L^2 under which the dynamics are stable, which then implies that the dynamics are also stable in L^2.

In the case that $m_k = 0$, the matrix in (3.5) has eigenvalues $\lambda = \pm ic$ each with geometric multiplicity of two, but yields the nontrivial Jordan form

$$\begin{bmatrix} -ic & 1 & 0 & 0 \\ 0 & -ic & 0 & 0 \\ 0 & 0 & ic & 1 \\ 0 & 0 & 0 & ic \end{bmatrix},$$

implying unstable growth of the perturbation like t. Finally, we note that if $m_k > 0$ (for any k), then the eigenvalues of S are purely real, so some of

the eigenvalues of (3.5) have a positive real part, again implying instability of the linear evolution problem. We summarize the above arguments as a pair of propositions which characterize the linear stability of the generalized Birkhoff-Rott Equation (3.1).

Proposition 3.1. *Define m_k as above for any $k \in \mathbb{N}$. If there exists an M so that $m_k < M < 0$ for all k, then the generalized Birkhoff-Rott equation is stable in $L^2(\mathbb{S})$ when linearized about the circular steady state.*

Proposition 3.2. *Define m_k as above for any $k \in \mathbb{N}$. If $m_k \geq 0$ for any k, then the generalized Birkhoff-Rott equation is unstable in $L^2(\mathbb{S})$ when linearized about the circular steady state.*

These results provide a direct characterization of linear instability/stability for general kernels. This characterization is made possible by both a decoupling between Fourier modes, which is also observed for the flat Kelvin-Helmholtz case. The characterization is also made possible by a relatively simple block structure of the matrix associated with each Fourier mode, allowing us to reduce checking stability of any given mode to computing a single, explicit constant.

In many cases it may be challenging compute m_k without resorting to numerical integration. Furthermore, the previous propositions did not directly account for the situation where $m_k \to 0$. It turns out that the popular kernel proposed in [21] has an exact integral identity that implies that $m_k \to 0$, independently of δ. In this case it turns out that we can still prove a linear instability result (with growth of the operator norm of order t), which we now state and prove.

Proposition 3.3. *The Krasny regularization of the generalized Birkhoff-Rott kernel is defined by*

$$K(z_1, z_2) = \frac{(z_1 - z_2)^*}{|z_1 - z_2|^2 + \delta^2}$$

for some $\delta > 0$. Under this kernel regularization, the generalized Birkhoff-Rott equation is unstable when linearized about the circular steady state, in the sense that the operator norm of the solution mapping grows at a rate proportional to t in $L^2(\mathbb{S})$.

Proof. The Krasny kernel regularization may be written as

$$\frac{(z_1 - z_2)^*}{f(|z_1 - z_2|)}$$

where $f(|z_1 - z_2|) = |z_1 - z_2|^2 + \delta^2$. We consider the evolution of a circular vortex sheet with a high-frequency perturbation, i.e. we define ξ by Equation (3.4) and take $k \to \infty$. Under integrability assumptions on f the terms M_4, M_5, M_6, and c all go to zero as $k \to \infty$. We are then left with $\lim_{k\to\infty} m_k =: m_\infty = (-M_1 + M_3)(M_1 + M_2)$.

To verify the asymptotic behavior of Equation (3.5) at high modes, we note that this is a linear evolution problem of the form $\frac{d}{dt}x_k(t) = A_k x_k(t)$, where the

matrix A_k is constant for a given k. It can be shown that for a fixed $t \in \mathbb{R}$, the matrix exponential $e^{A_k t} \to e^{A_\infty t}$ and thus the solution $x_k(t) \to x_\infty(t)$ as $A_k \to A_\infty$.

The integral $M_3 - M_1$ can be evaluated using trigonometric identities and substitutions as

$$\begin{aligned} M_3 - M_1 &= \frac{1}{2\pi}\int_0^{2\pi} \frac{f'(|1-e^{i\tilde{\beta}}|)}{f(|1-e^{i\tilde{\beta}}|)^2}\frac{\sin^2(\tilde{\beta})}{|1-e^{i\tilde{\beta}}|} - \frac{\cos(\tilde{\beta})}{f(|1-e^{i\tilde{\beta}}|)}d\tilde{\beta} \\ &= \frac{1}{2\pi}\int_0^{2\pi} \frac{2\sin^2(\tilde{\beta})}{(|1-e^{i\tilde{\beta}}|^2+\delta^2)^2} - \frac{\cos(\tilde{\beta})}{|1-e^{i\tilde{\beta}}|^2+\delta^2}d\tilde{\beta} \\ &= \frac{1}{2\pi}\int_0^{2\pi} \frac{2-(\delta^2+2)\cos(\tilde{\beta})}{(2(1-\cos(\tilde{\beta}))+\delta^2)^2}d\tilde{\beta} \\ &= \frac{\sin(\tilde{\beta})}{2\pi(2\cos(\tilde{\beta})-(\delta^2+2))}\Big|_0^{2\pi} = 0. \end{aligned}$$

We then have $m_\infty = 0$, which is the second case discussed in the section preceding Proposition 3.2. We conclude that the linear evolution problem is unstable for asymptotically high modes, in the sense that $\lim_{k\to\infty} \|e^{A_k}t\| \to Ct$ for any fixed t, where here A_k is the matrix associated with the k-th terms in the sine/cosine expansion, $\|\cdot\|$ here means the matrix norm, and C is independent of t. The fact that the Fourier series provides an orthonormal basis in L^2 then proves the desired result. □

For checking the stability of other kernel regularizations, it is useful to make a few further remarks about the structure of the matrix in (3.5):

i) Under integrability assumptions on f the terms M_4, M_5, M_6, and c all go to zero as $k \to \infty$. Hence, although we in principle need to compute the sign difference of the off-diagonals of S for all integer values of k, in practice a finite number of k will suffice.

ii) The off diagonal entries have terms $\pm(M_1 - M_4)$, so one can hope that these terms dominate the sign comparison. Indeed, M_1 has an integrand $\frac{\cos(\beta)}{f}$, and so the large values of $1/f$ near zero are not cancelled; a similar argument holds for M_4. Cancellation near zero does occur for all of the other terms.

4 Numerical Methods and Simulations

The analytical study of vortex sheet evolution is often limited by the approximations inherent in linearized analysis. Well-established numerical methods can help us understand nonlinear vortex sheet evolution up to and beyond the development of singularity [22, 23], for example illustrating the roll-up of Kelvin-Helmholtz on a flat sheet. We will focus on numerical methods for incompressible and inviscid dynamics.

4.1 Regularized Computational Method

The point vortex method is one such technique for computing vortex sheet evolution. Given a vortex sheet parameterized by vorticity, we consider the discretization $z_j = z(\alpha_j, t),\ j = 1, \ldots, N$. By approximating the sheet using point vortices at the points z_j, we can derive the system of ODEs [24]

$$\frac{dz_j^*}{dt} = \frac{1}{2\pi i} \sum_{k=1, k\neq j}^{N} K(z_j, z_k) w_k, \tag{4.1}$$

where the w_k are quadrature weights for the spatial discretization. A natural choice of kernel is

$$K(z_1, z_2) = \frac{1}{z_1 - z_2},$$

which is the kernel associated with the classical Birkhoff-Rott Equation (1.2), and in the discrete case it views vorticity as concentrated exactly at each z_j. Before the time of singularity development [30], the point vortex method with this kernel converges towards the Birkhoff-Rott solution as $N \to \infty$ [22]. After roll-up begins, the numerical evolution becomes unstable and kernel must be regularized to proceed further in time. One such regularization is the Krasny kernel [21]

$$K(z_1, z_2) = \frac{1}{z_1 - z_2} \frac{|z_1 - z_2|^2}{|z_1 - z_2|^2 + \delta^2},$$

which can be conveniently rewritten using properties of complex numbers as

$$K(z_1, z_2) = \frac{(z_1 - z_2)^*}{|z_1 - z_2|^2 + \delta^2}. \tag{4.2}$$

Here δ is a smoothing parameter which moderates the singularity in the Cauchy kernel; its presence corresponds to vorticity spread over small areas around each z_j. There are a variety of options for regularized kernels corresponding to the generalized Birkhoff-Rott Equation (3.1), also including the α-regularization studied by [4] which may be written in complex coordinates as

$$K(z_1, z_2) = \frac{1}{z_1 - z_2} \left(1 - \frac{|z_1 - z_2|}{\alpha} K_1 \left(\frac{|z_1 - z_2|}{\alpha} \right) \right) \tag{4.3}$$

In Equation (4.3), K_1 denotes a modified Bessel function of the second kind of order one. Throughout this work, we will a standard Runge-Kutta method to solve the system of ODEs given by the chosen kernel regularization and Equation (4.1).

4.2 Nonlinear Simulation

To illustrate the effectiveness of the regularized point-vortex method, we first use (4.2) to simulate the Kelvin-Helmholtz instability on an initially flat sheet

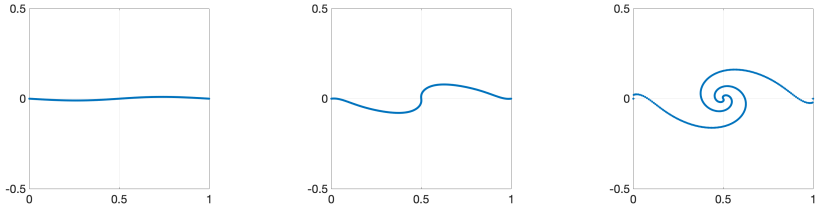

(a) $t = 0$ (b) $t = 1$ (c) $t = 1.5$

Figure 2: The Kelvin-Helmholtz instability on a flat sheet.

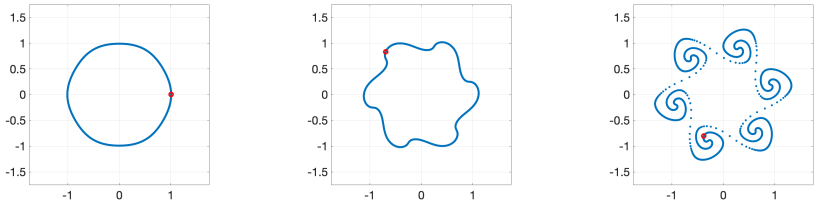

(a) $t = 0$ (b) $t = 5$ (c) $t = 10$

Figure 3: Nonlinear evolution of a perturbed circular vortex sheet.

with a periodic perturbation of the form $z(\alpha, 0) = \alpha + \xi(\alpha, 0)$. We apply periodic boundary conditions, implemented as described in [21]. Mirroring that study, we use $\delta = 0.25$ and $N = 400$ with the initial condition $z(\alpha, 0) = \alpha + 0.01 \sin(2\pi\alpha) - i0.01 \sin(2\pi\alpha)$ for $\alpha \in [0, 1]$. Figure 2 shows the computed evolution.

The roll-up observed here is characteristic of the Kelvin-Helmholtz instability [11, 24] and is a classical problem in computing vortex sheet motion. It is important to note that although linearized analysis of the flat vortex sheet indicates some strong instability, it does not capture a mechanism for the roll-up observed numerically and experimentally. The influence of the smoothing parameter δ is discussed in detail in [21]; smaller values of δ lead to an increased number of turns observed in the core of the roll-up at a given time, and the kernel approaches that of the classical Birkhoff-Rott equation, but introduces challenges at finite precision.

We can similarly use the regularized point-vortex method with the Krasny kernel (4.2) to simulate the evolution of an initially circular vortex sheet with a periodic perturbation of the form $z(\alpha, 0) = e^{i\alpha}(1 + \xi(\alpha, 0))$. Since the geometry is a closed contour, there is no need to apply a periodic boundary condition and the numeric evolution can be viewed purely as an initial value problem. We use $\delta = 0.25$, $N = 1600$, and the initial condition $z(\alpha, 0) = e^{i\alpha}(1 + 0.01 \cos(6\alpha))$. Figure 3 shows the computed evolution.

The perturbed circular vortex sheet exhibits nonlinear instability by rolling

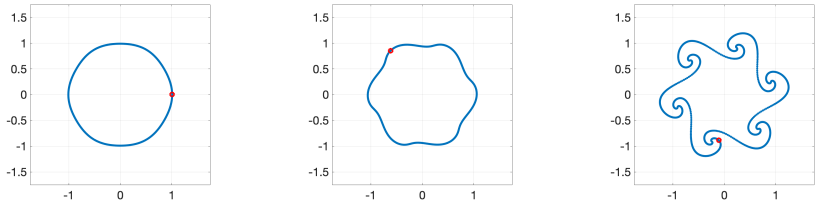

(a) $t = 0$ (b) $t = 5$ (c) $t = 10$

Figure 4: Nonlinear evolution of a perturbed circular vortex sheet with the α-regularized kernel.

up much like the Kelvin-Helmholtz instability on a flat vortex sheet, albeit more slowly. In particular, roll-up solutions on both circular and flat sheets exhibit wave breaking phenomena, in the sense that solutions of the nonlinear equations cease to be the graph of a (real-valued) function ξ.

This instability is expected from our analysis of the generalized Birkhoff-Rott equation in Section 3. In particular, Proposition 3.3 proved linearized instability for the Krasny kernel under high-frequency perturbations. Here, we observe nonlinear instability under a relatively low-frequency perturbation.

To demonstrate that this wave-breaking phenomena is consistent across regularizations of the kernel, we simulate the perturbed circular vortex sheet with the same initial condition $z(\alpha, 0) = e^{i\alpha}(1 + 0.01\cos(6\alpha))$. We apply the point-vortex method with the α-regularized kernel (4.3). To avoid confusing notation we regularize with the variable δ, setting $\delta = 0.25$ and $N = 1600$. Figure 4 shows the computed evolution.

Though instability develops more slowly than with the Krasny kernel, the same wave-breaking instability is clearly observed. As for the Krasny kernel, decreasing the magnitude of the smoothing parameter leads to more turns observed in the core of the roll-up at a given time. Figures 3 and 4 suggest that the wave-breaking instability is robust under variation of the regularizing kernel. This observation could be validated analytically using the tools developed in Section 3.

5 Experimental Demonstration

Experimentation was used to qualitatively demonstrate the development of instability on a circular shear layer, providing a compelling physical validation of some patterns we observed numerically. Existing research has shown that under the influence of centrifugal forces, a stable circular shear layer may be observed with steady polygonal patterns of vortices [1, 16]. This contour corresponds to our perturbed circular vortex sheet. Since the linearized evolution of such a vortex sheet under the classical Birkhoff-Rott equation is shown here

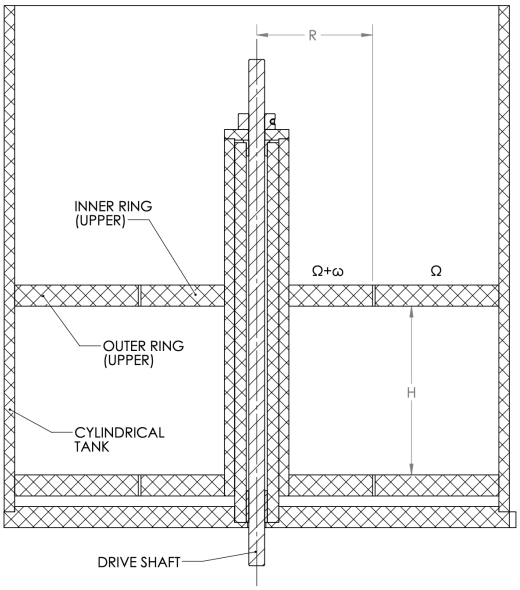

Figure 5: Experimental setup, with test section height H and split radius at R.

to be stable, but regularized numerical simulations indicate a wave-breaking instability, it was reasonable to assume that the presence of background rotation was stabilizing. Such an effect also explains why [38] obtained steady polygonal patterns. Thus, our procedure will isolate the development of instability by removing background rotation once a steady flow is established.

5.1 Experimental Design

The experimental setup broadly consists of a large acrylic cylinder with a differentially rotating core. The test section is defined by acrylic annuli offset at height H. The outer annuli are fixed to the wall of the tank. At the upper and lower boundary of the test section, two inner annuli of radius R rotate with the central core at speed ω, driven by a motor underneath the tank. The cylinder is filled with water to a level slightly above the upper annuli. Figure 5 shows a vertical cross-section.

Placing the experimental setup on a variable speed turntable permits the outer section to rotate at speed Ω and the inner section at speed $\Omega + \omega$, establishing a vertical shear layer between the flow regions at radius R. The parameters used to describe the dynamics are the Ekman number E and Rossby number Ro. In their definition, ν is the kinematic viscosity of the working fluid and $\overline{\Omega}$ is the mean fluid velocity, calculated using the area ratio of inner and outer annuli. The parameters are calculated as

Variable	Value/range
Overall dia.	11.5 in.
Inner core rad.	0.75 in.
H	2.06 in.
R	2.75 in.
ν	0.0016 in^2/s (water at 20°C)
Ω	$-75 \leq \Omega \leq 75$ rpm $\pm 0.05\%$
ω	3 or 6 rpm $\pm 0.05\%$

Table 1: Experimental variables.

$$E = \frac{\nu}{\overline{\Omega} H^2}, \tag{5.1}$$

$$Ro = \frac{R\omega}{2\overline{\Omega} H}. \tag{5.2}$$

For $\Omega \neq 0$ and $\omega \neq 0$, viscous forces lead to the formation of horizontal shear layers, called Ekman layers, of radius R against the upper and lower boundaries of the test section. The thickness of the Ekman layers are proportional to $E^{1/2}$. A vertically uniform Stewartson shear layer of height H and thickness $L = (E/4)^{1/4}H$ forms at the split radius; for sufficiently small E this cylindrical shear layer approximates the circular vortex sheet when viewed from above [16, 39].

A complication of [38] in their attempt to study the onset of instability on a circular vortex sheet was to set H so small that the observed dynamics took place inside the horizontal Ekman layer [38]. Though the team established an approximately circular geometry similar to [1, 16], the excessive strength of viscous effects in the Ekman layer likely obscured the dynamics as represented by the Birkhoff-Rott equation. Our experiment therefore employed the values presented in Table 1; the geometry is a scaled version of that used in [1, 16], which met our experimental constraints and allows a larger value of H to permit visualization of the dynamics outside the Ekman layer.

By varying Ω and ω, we established approximately circular contours with symmetric polygonal patterns of m vortices. A thorough regime diagram over Ro and E has been constructed by both [1] and [16] which shows how different parameter choices lead to different steady state values of m in the case of background rotation. Since our goal is to study the development of instability rather than steady states, we restricted our attention to a smaller range of parameter values as described in Section 5.2.

Our experimental procedure used the background rotation Ω to stabilize the circular shear layer at some value of m, so the flow structure corresponds to physical perturbations of the circular solution to Birkhoff-Rott. After observing the steady state, background rotation was removed while keeping the velocity differential ω constant, triggering the onset of instability at inflection points.

This approach focuses on the development of instability and thus avoids the other potential problem with [38], which by attempting to produce a permanent shear layer obtained a steady flow structure dependent on background rotation rather than the Kelvin-Helmholtz instability.

We conducted all experimental trials using $\omega = 3$ or 6 rpm and various values of Ω. For each trial, the test setup was filled with water to slightly above the upper annuli. The motors were turned on and their speeds measured with a handheld tachometer, which has a relative precision of $\pm 0.05\%$. The flow was then allowed to equilibriate for 30 minutes. At this point a steady flow had been established, so ω and Ω were measured again and visualization could proceed. The flow was visualized using fluorescein dye, which was injected by hand at the split radius.

Since the dye diffused within a few minutes, two trials needed to be conducted for each steady state. In the first trial, the steady state was visualized by injecting the dye with $\Omega \neq 0$. Once we understood the steady state from which instability would develop, the water was refreshed and a second trial was equilibriated under identical conditions. In the second trial, we set $\Omega = 0$ and then immediately injected dye to visualize the breakdown of the previously observed shear layer. We note that this experimental constraint introduces some degree of uncertainty.

5.2 Primary Experimental Results

In this section we present qualitative results and compare them with numerical simulation of the inviscid model. This experiment focuses on the steady state and development of instability for a particular polygonal configuration of vortices with $m = 3$, because this configuration was the simplest to obtain within the constraints of our test setup.

The most interesting case is with $\omega = 6.0$ and $\Omega = 31.0$ rpm, so that $Ro = 0.12$ and $E = 1.1 \times 10^{-4}$. These conditions lead to the development of a steady shear layer containing $m = 3$ vortices. Figure 6 shows the steady state.

Interestingly, [1, 16] both achieved $m = 4$ or 5 for the same parameters. Similar discrepancies emerged for other parameter values, which suggests that either the dynamics depend on the scale of the test setup, or there may be a more descriptive parameter choice to describe the flow.

The development of instability under identical conditions to Figure 6 is shown by the series of images in Figure 7.

Numerical simulation of the inviscid analog is shown in Figure 8. Starting with the initial condition $z(\alpha, 0) = e^{i\alpha}(1 + 0.1\cos(3\alpha))$, we implement the regularized point vortex method Eq. (4.1) and (4.2) with $\delta = 0.25$ and $N = 800$.

The qualitative similarities between Figures 7 and 8 are striking. The most notable feature is the development of a wave-breaking instability with symmetry $m = 3$ corresponding to the symmetry of the initial condition. Behind each

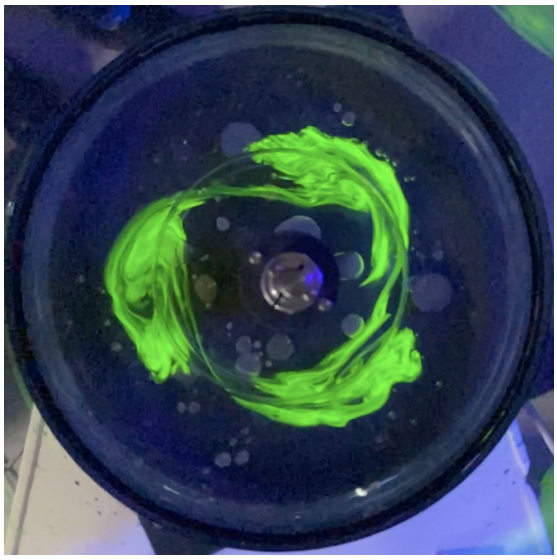

Figure 6: Steady state with $Ro = 0.12$ and $E = 1.1 \times 10^{-4}$, $m = 3$ vortices are visible.

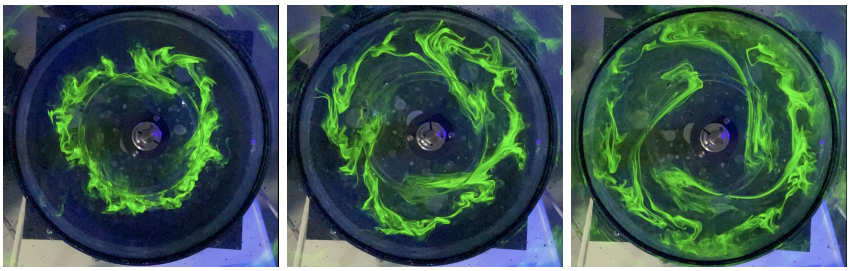

(a) $t = 0$s (b) $t = 55$s (c) $t = 127$s

Figure 7: Development of instability for $Ro = 0.12$ and $E = 1.1 \times 10^{-4}$, with $m = 3$.

rolled-up vortex is an extended tail. Viscous effects are identifiable in the tendency of the real vortex sheet to increase in diameter over time, and its eventual interaction with the outer wall of the tank, but the experiment is nonetheless a convincing verification of our numerical model and the anticipated behavior.

5.3 Auxiliary Results

Reversing the velocity differential was accomplished by setting $\Omega < 0$. Employing similar parameter magnitudes to the main case discussed above resulted in a very similar instability phenomenon with $m = 3$ vortices in the steady state and breakdown, indicating that the observed instability is not heavily dependent on

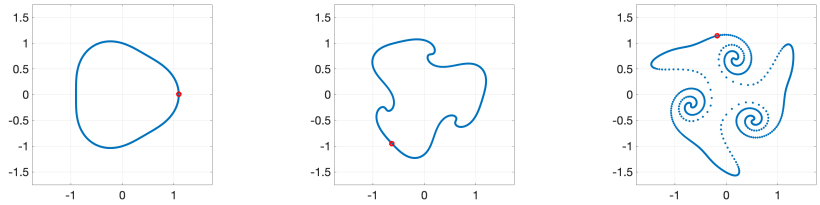

(a) $t = 0$ (b) $t = 5$ (c) $t = 10$

Figure 8: Simulated development of instability for $m = 3$.

the direction of the velocity differential.

Several approaches are possible to achieve different values of m. Due to physical constraints of our experimental setup the best way to explore the parameter space was with a smaller value of ω, which decreases the magnitude of the velocity differential. In lieu of a complete regime diagram, Table 2 presents a small collection of parameter values and the order of symmetry observed in the steady state.

Ω (rpm)	ω (rpm)	Ro	E	Symmetry m
-31.0	6.0	-0.13	-1.1×10^{-4}	3
31.0	6.0	0.12	1.1×10^{-4}	3
17.8	3.2	0.12	1.9×10^{-4}	3
31.0	3.5	0.07	1.1×10^{-4}	4
49.5	3.5	0.05	7.0×10^{-5}	5 (irregular)

Table 2: Effect of parameter variation on observed steady-state symmetry.

It is evident that decreasing the magnitude of parameter values, especially the Rossby number, leads to the development of higher orders of symmetry in the steady state. This trend is consistent with [1, 16], though the parameter values obtained here correspond to different slightly values of m than observed in those studies. It is also noted that the observation of higher values of m was limited by the method of injecting dye by hand, which is not very precise when the vortex sheet approaches circular.

In our analytical work and numerical simulations, the strength of the vortex sheet does not affect the dynamics because a time transformation can be easily performed in the inviscid case. However in the real viscous case, decreased magnitude of the velocity differential plays an important role in the dynamics. Though similar steady-state geometries can be achieved with a smaller velocity differential, viscous effects dominate the destabilizing vortex sheet by causing the contour to increase in diameter more rapidly than wave-breaking instability forms, curtailing observation of similarities between experiments and simulations.

6 Conclusion

This article suggests that the linear stability of the Birkhoff-Rott equation depends strongly on the geometry of the vortex sheet. In Section 2.1, we presented a classical linearized analysis of the Kelvin-Helmholtz instability on a flat sheet. We then proved that the Birkhoff-Rott equation is linearly stable for an initially circular geometry. This result suggests that classical linear dynamics are insufficient for explaining the wave-breaking instability observed in numerical simulations, and motivates the study of regularizing kernels for the generalized Birkhoff-Rott equation. In Section 3, we establish a simple criterion for evaluating the linearized stability of circular sheet under regularizing kernels. Counterintuitively, we proved that the addition of a smoothing parameter in the Krasny kernel leads to linearized instability. In Section 4, we presented numerical demonstrations of vortex sheet instability, which included validation for the instability of the Krasny kernel. Finally, physical experiments offered a qualitative validation of our numerical model by demonstrating the wave-breaking instability that model predicted.

7 Acknowledgements

The experimental portion of this research project was made possible by funding from the North Carolina State University Office of Undergraduate Research and the support of Dr. Mark Pankow in the Department of Mechanical and Aerospace Engineering. The authors would also like to thank Zach Berger and Ayman Said for many helpful discussions.

References

[1] Ana C. Barbosa Aguiar, Peter L. Read, Robin D. Wordsworth, Tara Salter, and Y. Hiro Yamazaki. A laboratory model of saturn's north polar hexagon. *Icarus*, 206:755–763, 2010.

[2] K. Baines, Thomas Momary, Leigh Fletcher, Joo Hyeon Kim, A. Showman, S. Atreya, R. Brown, B. Buratti, R. Clark, and P. Nicholson. Saturn's north polar region at depth: The north polar hexagon and north polar cyclone observed over two years by cassini/vims. *Geophys. Res. Abstr.*, 11:3375, 03 2009.

[3] Claude Bardos and David Lannes. Mathematics for 2d interfaces. *arXiv preprint arXiv:1005.5329*, 2010.

[4] Claude Bardos, Edriss S Titi, and Jasmine S Linshiz. Global regularity and convergence of a birkhoff-rott-α approximation of the dynamics of vortex sheets of the two-dimensional euler equations. *Communications on Pure and Applied Mathematics: A Journal Issued by the Courant Institute of Mathematical Sciences*, 63(6):697–746, 2010.

[5] George Keith Batchelor. *An Introduction to Fluid Dynamics*. Cambridge University Press, 2000.

[6] Ricardo Abreu Blaya, Juan Bory Reyes, and Boris Aleksandrovich Kats. Cauchy integral and singular integral operator over closed jordan curves. *Monatshefte für Mathematik*, 176:1–15, 2015.

[7] Alberto Bressan and Ryan Murray. On self-similar solutions to the incompressible euler equations. *Journal of Differential Equations*, 269(6):5142–5203, 2020.

[8] Russel E Caflisch and Oscar F Orellana. Singular solutions and ill-posedness for the evolution of vortex sheets. *SIAM Journal on Mathematical Analysis*, 20(2):293–307, 1989.

[9] Tomasz Cieślak, Piotr Kokocki, and Wojciech S Ożański. Well-posedness of logarithmic spiral vortex sheets. *arXiv preprint arXiv:2110.07543*, 2021.

[10] Tomasz Cieślak, Piotr Kokocki, and Wojciech S Ożański. Existence of non-symmetric logarithmic spiral vortex sheet solutions to the 2d euler equations. *arXiv preprint arXiv:2207.06056*, 2022.

[11] Philip G Drazin and William Hill Reid. *Hydrodynamic stability*. Cambridge university press, 2004.

[12] Jean Duchon and Raoul Robert. Global vortex sheet solutions of euler equations in the plane. *Journal of Differential Equations*, 73(2):215–224, 1988.

[13] V Elling and MV Gnann. Variety of unsymmetric multibranched logarithmic vortex spirals. *European Journal of Applied Mathematics*, 30(1):23–38, 2019.

[14] Volker Elling. Algebraic spiral solutions of the 2d incompressible euler equations. *Bulletin of the Brazilian Mathematical Society*, 47(1), 2016.

[15] Volker Elling. Self-similar 2d euler solutions with mixed-sign vorticity. *Communications in Mathematical Physics*, 348(1):27–68, 2016.

[16] Wolf-Gerrit Fruh and Peter L. Read. Experiments on a barotropic rotating shear layer. part 1. instability and steady vortices. *J. Fluid Mech.*, 383:143–173, 1999.

[17] D.A. Godfrey. A hexagonal feature around saturn's north pole. *Icarus*, 76:335–356, 1988.

[18] Loukas Grafakos. *Modern Fourier Analysis*. Graduate Texts in Mathematics. Springer, 2014.

[19] Heinrich Kaden. Aufwicklung einer unstabilen unstetigkeitsfläche. *Ingenieur-Archiv*, 2(2):140–168, 1931.

[20] Theodore Kolokolnikov, Hui Sun, David Uminsky, and Andrea L Bertozzi. Stability of ring patterns arising from two-dimensional particle interactions. *Physical Review E*, 84(1):015203, 2011.

[21] R. Krasny. Desingularization of periodic vortex sheet roll-up. *J. Computational Physics*, 65:292–313, 1986.

[22] Robert Krasny. A study of singularity formation in a vortex sheet by the point-vortex approximation. *Journal of Fluid Mechanics*, 167:65–93, 1986.

[23] Robert Krasny. Computing vortex sheet motion. In *Proc. of Inte. Cong. Math., Kyoto, Japan*, pages 1573–1583, 1990.

[24] Robert Krasny. Lagrangian simulation of vortex sheet dynamics. 05 2008.

[25] Gilles Lebeau. Régularité du problème de kelvin–helmholtz pour l'équation d'euler 2d. *ESAIM: Control, Optimisation and Calculus of Variations*, 8:801–825, 2002.

[26] Jian-Guo Liu and Zhouping Xin. Convergence of vortex methods for weak solutions to the 2-d euler equations with vortex sheet data. *Communications on Pure and Applied Mathematics*, 48(6):611–628, 1995.

[27] Milton Lopes Filho, Helena Nussenzveig Lopes, and Steven Schochet. A criterion for the equivalence of the birkhoff-rott and euler descriptions of vortex sheet evolution. *Transactions of the American Mathematical Society*, 359(9):4125–4142, 2007.

[28] Andrew J. Majda and Andrea L. Bertozzi. *Vorticity and Incompressible Flow.* Cambridge Texts in Applied Mathematics. Cambridge University Press, 2002.

[29] Alfons Michalke and Adalbert Timme. On the inviscid instability of certain two-dimensional vortex-type flows. *Journal of Fluid Mechanics*, 29(4):647–666, 1967.

[30] D. W. Moore. The spontaneous appearance of a singularity in the shape of an evolving vortex sheet. *Proceedings of the Royal Society of London. Series A, Mathematical and Physical Sciences*, 365(1720):105–119, 1979.

[31] D.W. Moore. Numerical and analytical aspects of helmholtz instability. In *Theoretical and applied mechanics*, pages 263–274. Elsevier, 1985.

[32] Max Munk. *Isoperimetrische Aufgaben aus der Theorie des Fluges.* Dieterichsche Universitäts-Buchdruckerei, 1919.

[33] Monika Nitsche, Mark A Taylor, and Robert Krasny. Comparison of regularizations of vortex sheet motion. In *Computational Fluid and Solid Mechanics 2003*, pages 1062–1065. Elsevier, 2003.

[34] Bartosz Protas and Takashi Sakajo. Rotating equilibria of vortex sheets. *Physica D: Nonlinear Phenomena*, 403:132286, 2020.

[35] Bartosz Protas, Stefan G Llewellyn Smith, and Takashi Sakajo. Finite rotating and translating vortex sheets. *Journal of Fluid Mechanics*, 923, 2021.

[36] D.I. Pullin. The large-scale structure of unsteady self-similar rolled-up vortex sheets. *Journal of Fluid Mechanics*, 88(3):401–430, 1978.

[37] D.I. Pullin and W.R.C. Phillips. On a generalization of kaden's problem. *Journal of Fluid Mechanics*, 104:45–53, 1981.

[38] M. Rabaud and Y. Couder. A shear-flow instability in a circular geometry. *J. Fluid Mech.*, 136:291–319, 1983.

[39] K Stewartson. On almost rigid rotations. *Journal of Fluid Mechanics*, 3(1):17–26, 1957.

[40] Hui Sun, David Uminsky, and Andrea L Bertozzi. A generalized birkhoff–rott equation for two-dimensional active scalar problems. *SIAM Journal on Applied Mathematics*, 72(1):382–404, 2012.

[41] Sijue Wu. Recent progress in mathematical analysis of vortex sheets. *Proceedings of the ICM*, 3:233–242, 2003.

[42] Sijue Wu. Mathematical analysis of vortex sheets. *Communications on Pure and Applied Mathematics: A Journal Issued by the Courant Institute of Mathematical Sciences*, 59(8):1065–1206, 2006.